

Supplementary Material for

# **On the Cause of Large Daily River Flow Fluctuations in the Mekong River**

Khosro Morovati<sup>1,2</sup>, Lidi Shi<sup>3</sup>, Yadu Pokhrel<sup>4</sup>, Maozhu WU<sup>1</sup>, Paradis Someth<sup>5</sup>, Sarann Ly<sup>6</sup>,  
Fuqiang Tian<sup>\*1,2</sup>

<sup>1</sup>Department of Hydraulic Engineering & State Key Laboratory of Hydro-science and Engineering, Tsinghua University, Beijing, 100084, China

<sup>2</sup>Key Laboratory of Hydrosphere Sciences of the Ministry of Water Resources, Tsinghua University, Beijing, 100084, China

<sup>3</sup>Department of Physical and Environmental Sciences, University of Toronto Scarborough, Toronto, Ontario, Canada

<sup>4</sup>Department of Civil and Environmental Engineering, Michigan State University, East Lansing, 48823, United States

<sup>5</sup>eWater, UC Innovation Centre, University Drive South, Canberra, Australian Capital Territory, 2617, Australia.

<sup>6</sup>Mekong River Commission Secretariat (MRCS), Technical Support Division, Vientiane 01000, Lao PDR.

*Correspondence to:* Fuqiang Tian ([tianfq@mail.tsinghua.edu.cn](mailto:tianfq@mail.tsinghua.edu.cn))

## The Supplementary Material contains the following items:

1. Additional information for developed hydrodynamic model
2. A figure for the storage of tributary dams
3. Bathymetry data
4. Additional figures for the developed hydrodynamic model
5. Additional figures for the THREW hydrological model
6. Additional figures for large water level/flow changes
7. Additional figures for the contribution of sub-basins to mainstream flow
8. Additional figures for each event resulting in daily water level increases for all stations
9. A figure for the precipitation trend

### 1. Additional information for developed hydrodynamic model

#### 1.1 Numerical set-up

The impermeable riverbed was addressed by setting the vertical velocity relative to the reference planes to zero. Following this, the subsequent boundary conditions were defined for the momentum equations in the following manner:

$$\left(\frac{u_v}{H} \frac{\partial u}{\partial \sigma}\right)_{\sigma=-1} = \frac{1}{\rho_0} \tau_{b\zeta} \quad \text{and} \quad \left(\frac{u_v}{H} \frac{\partial v}{\partial \sigma}\right)_{\sigma=-1} = \frac{1}{\rho_0} \tau_{b\xi} \quad (1)$$

where  $\tau_{b\zeta}$  and  $\tau_{b\xi}$  represent the components of the bed stress.

The two-equation model, referred to as the  $k - \varepsilon$  turbulence model, enables the separate calculation of  $k$  and  $\varepsilon$  using Equations 2 and 3, respectively. Within this model, the production and dissipation terms are the primary factors. Additionally, the vertical length scales are noted to be smaller than their horizontal counterparts.

$$\frac{\partial k}{\partial t} + \frac{u}{R \cos \phi} \frac{\partial k}{\partial \lambda} + \frac{v}{R} \frac{\partial k}{\partial \eta} + \frac{w}{d + \partial \sigma} \frac{\partial k}{\partial \sigma} = \frac{1}{(d + \zeta)^2} \frac{\partial}{\partial \sigma} \left( D_k \frac{\partial k}{\partial \sigma} \right) + P + P + B - \varepsilon \quad (2)$$

$$\frac{\partial \varepsilon}{\partial t} + \frac{u}{R \cos \phi} \frac{\partial \varepsilon}{\partial \lambda} + \frac{v}{R} \frac{\partial \varepsilon}{\partial \eta} + \frac{w}{d + \zeta} \frac{\partial \varepsilon}{\partial \sigma} = \frac{1}{(d + \zeta)^2} \frac{\partial}{\partial \sigma} \left( D_\varepsilon \frac{\partial \varepsilon}{\partial \sigma} \right) + P_\varepsilon + P_{\partial w} - B_\varepsilon - c_{2\varepsilon} \frac{\varepsilon^2}{k} \quad (3)$$

#### 1.2 Meshing

Splines were delineated along the land boundaries, aligned with the flow path. The meshing of the computational domain was executed to meet the smoothness and orthogonality requirements of the spherical system. A 3D mesh was generated in spherical coordinates for the computational domain, comprising 10 layers for river depth, which remained constant for the river length representing each sub-basin. For the river width, the same number of cells (50 cells) was employed from JingHong to Kratie stations, as the computational domain in the river width direction remained unchanged at 2 km. In contrast, for the river length, since each sub-basin was simulated independently, the number of cells varied according to the river length of each sub-basin; nevertheless, the cell length remained constant at 60 m.

## 2. A figure for the storage of tributary dams

Attributes for all tributary dams are not available. Figure S1 shows the total storage capacity for 83 tributary dams. Xe Kaman and Nam Ngum tributary dams located in Lao PDR have the highest storage capacity than other dams, with 4.8 km<sup>3</sup> and 4.7 km<sup>3</sup>, respectively.

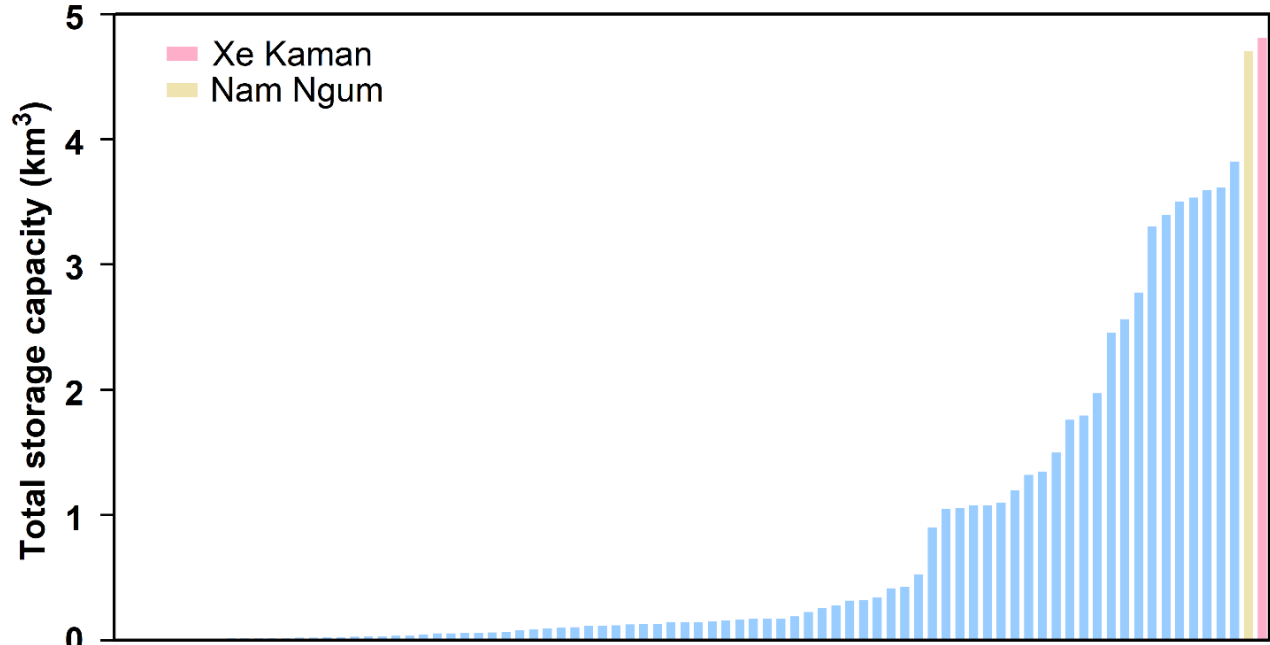


Figure S1: Illustrates of the total storage capacity of tributary dams along the Mekong River. Please note that attributes for all tributary dams are not available, and this figure represents data solely for the available dams.

## 3. Bathymetry

While the lower Mekong generally exhibits placid conditions, the depth representation may vary across the river, potentially impacting flow dynamics. As such, reliable bathymetry data are essential. For the surrounding areas, data from the Shuttle Radar Topography Mission (SRTM) with an original resolution of 90 meters were employed. However, the density of this bathymetry data was insufficient compared to the resolution of the defined mesh. To address this, interpolation using the triangular technique was employed, supplemented by the internal diffusion method to assign depths to non-interpolated areas (refer to Deltares, 2014 for detailed information).

For the river, cross-sectional shapes were available at various stations, and an anisotropy approach was adopted during depth interpolation due to its superior performance in the flow-oriented coordinate system (see Merwade et al., 2006). To replicate digital elevation models (DEMs) in areas lacking bathymetry data, the RGFGRID tool integrated into Delft3D-Flow was utilized to establish an orthogonal grid system (refer to Deltares, 2014).

Figure S2 illustrates a comparison between the predicted cross-section at the Pakse (PA) station and the measured cross-section. It is evident that, although there are some discrepancies, the overall shape of the predicted cross-section closely resembles that of the measured one.

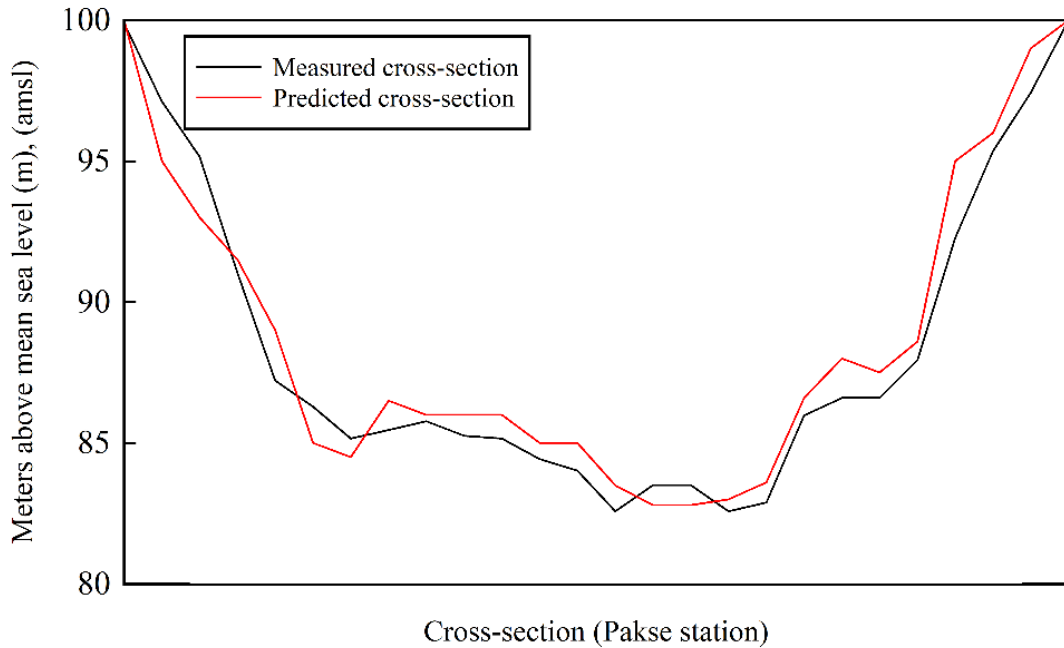


Figure S2: A comparison between the measured bed profile and the predicted profile at the Pakse (PA) station.

#### 4. Additional figures for the developed hydrodynamic model

Fig. S2 illustrates the comparison between the velocity profiles obtained from the hydrodynamic model and the measured values for the years 2019 and 2020 at the Stung Treng station. A detailed point-by-point comparison indicates a relatively high level of accuracy, with mean relative errors of 5.5% and 6.2% for the data from 2019 and 2020, respectively.

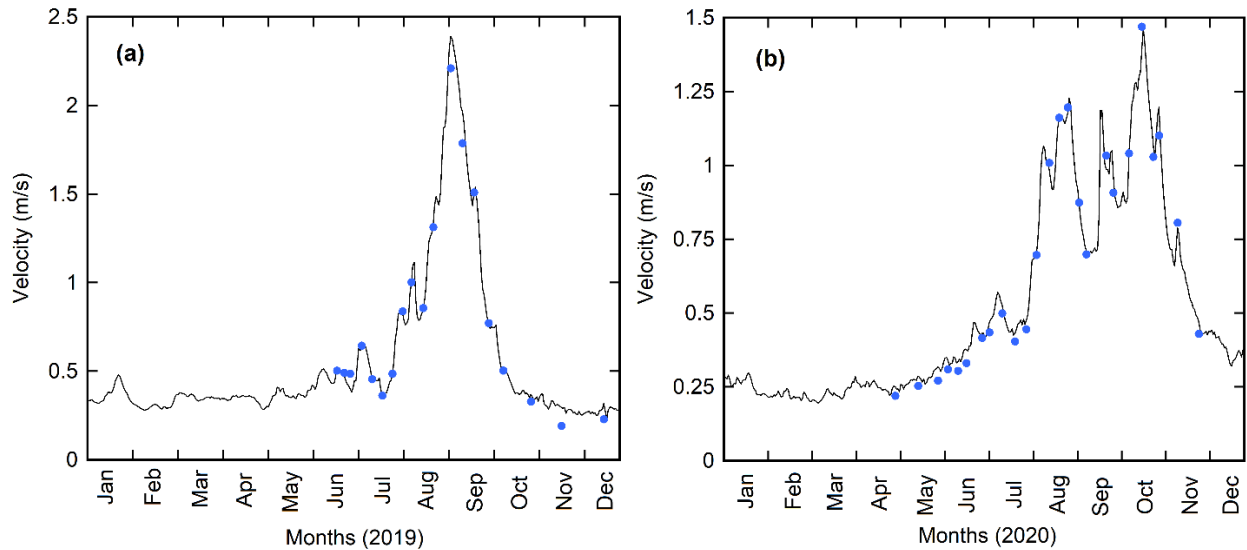


Figure S3: A point-by-point comparison of measured velocity data with hydrodynamic model for the years 2019 (part a) and 2020 (part b) at Stung Treng station.

The comparison between water levels yielded by the hydrodynamic model and the measured ones demonstrates a high level of accuracy, with an NSE exceeding 0.94. The model accurately captures both high and low flows throughout the wet and dry seasons.

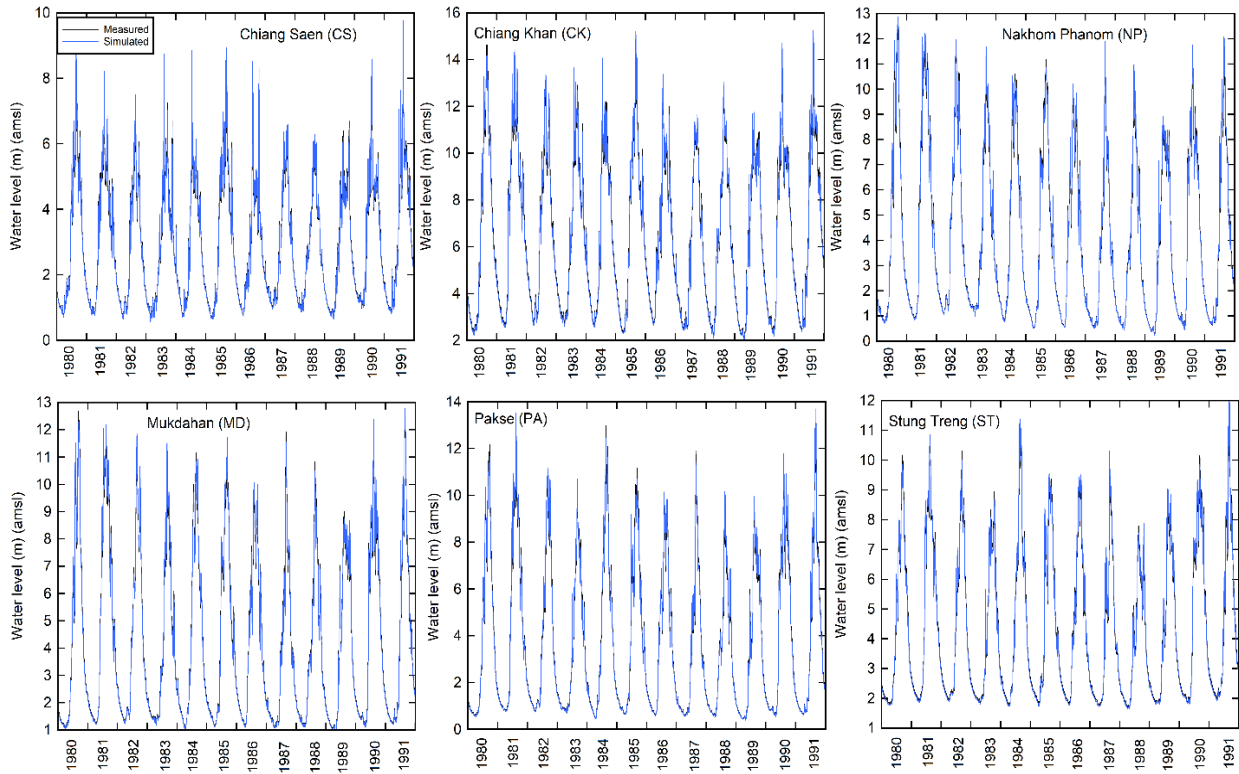


Figure S4: A comparison of measured water levels with those obtained by the hydrodynamic model for mainstream stations.

### 5. Additional figures for the THREW hydrological model

Figure S5 shows the discharge data produced for six tributary stations along the Mekong River, utilizing the THREW hydrological model. It is evident from the figures that the model has captured both high and low-flow events across various years. The NSE values, indicating model performance, are consistently high, surpassing 0.88.

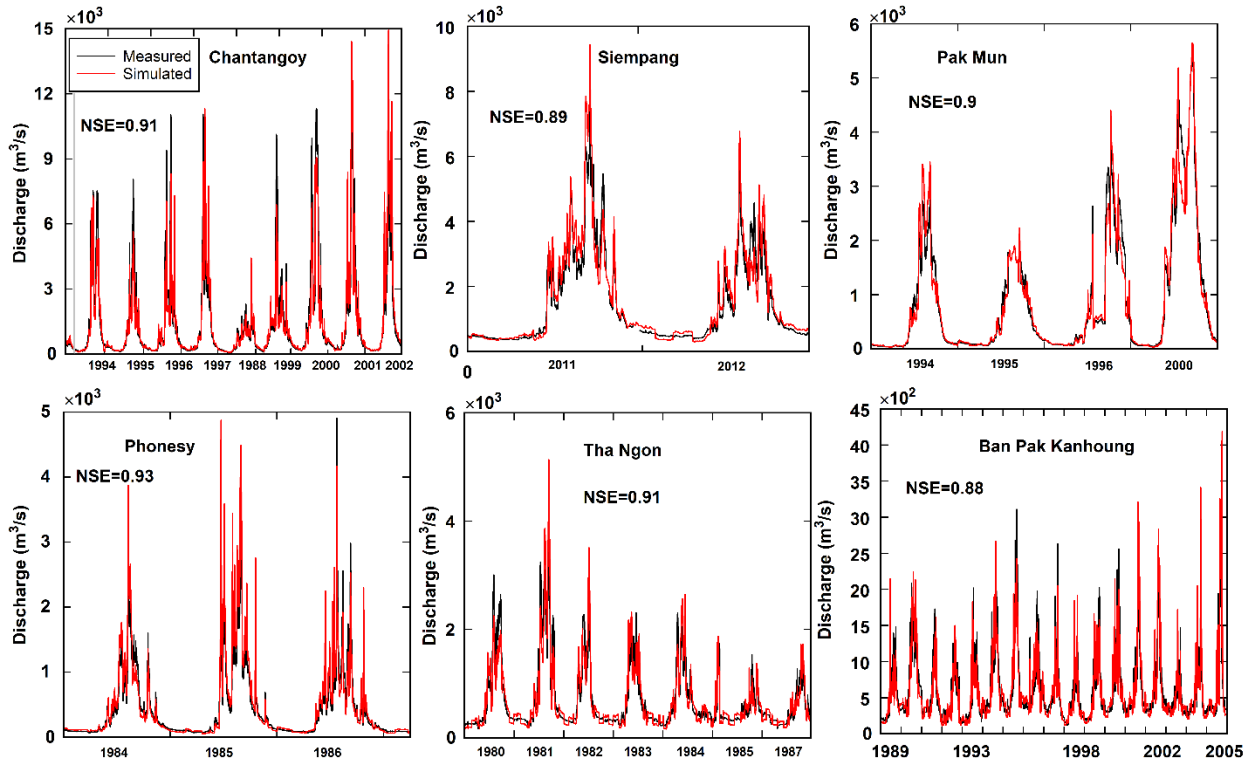
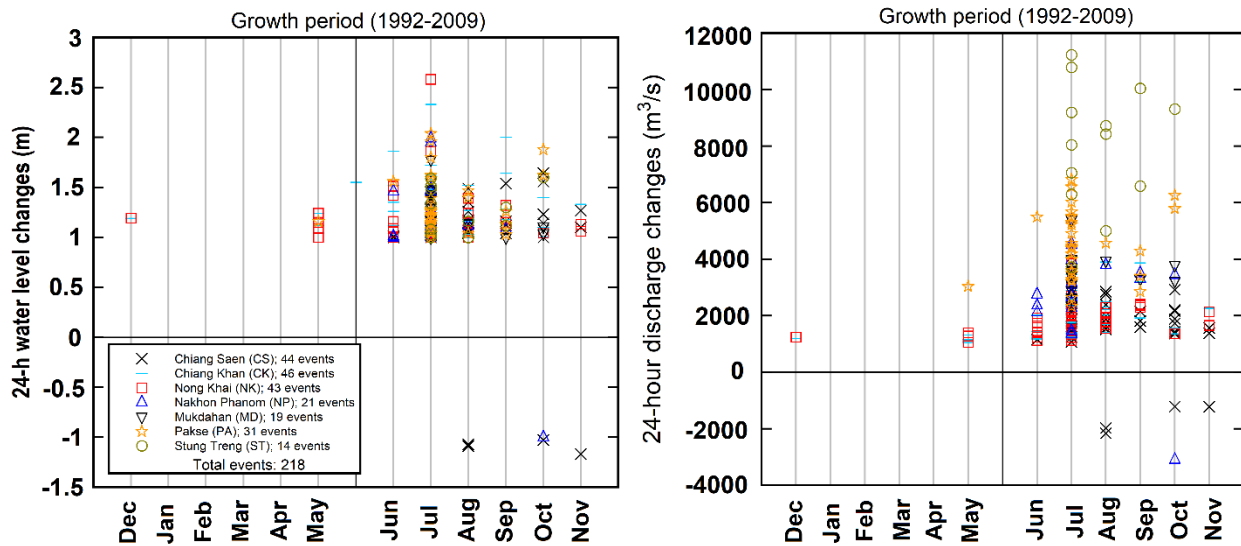


Figure S5. Comparison of the produced discharge data using the THREW hydrological model at tributaries across the Mekong River with measured data.

## 6. Additional figures for large water level/flow changes



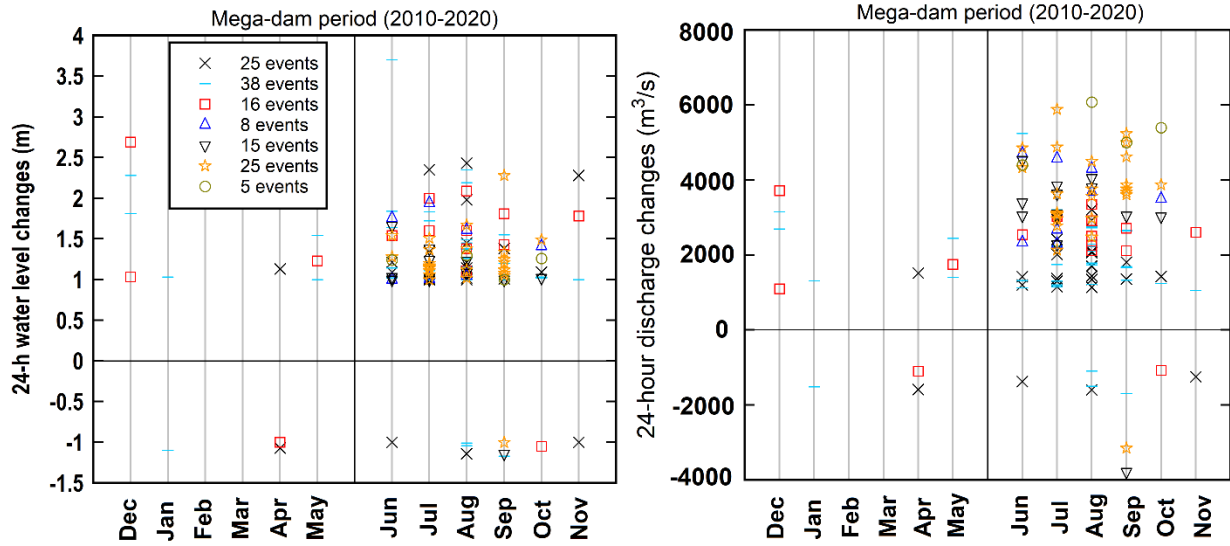


Figure S6. Large daily water level/flow changes during the mega-dam and growth periods for all mainstream stations.

### 6. Additional figures for the contribution of sub-basins to mainstream flow

Figure S7 illustrates the contribution of each sub-basin and upstream station to the total discharge passing through each station. While a nearly identical contribution is observed compared to the pre-dam period, there has been a reduction in the total discharge passing through mainstream stations during the mega-dam period compared to the two previous periods. For instance, at Stung Treng (ST) station, the mean discharge during the wet season decreased by approximately 5.1%, and during the dry season by about 10.7% in the mega-dam period compared to the pre-dam period, resulting in a reduction from 24,130 m<sup>3</sup>/s to 22,896 m<sup>3</sup>/s during the wet season and from 4,849 m<sup>3</sup>/s to 4,326 m<sup>3</sup>/s during the dry season.

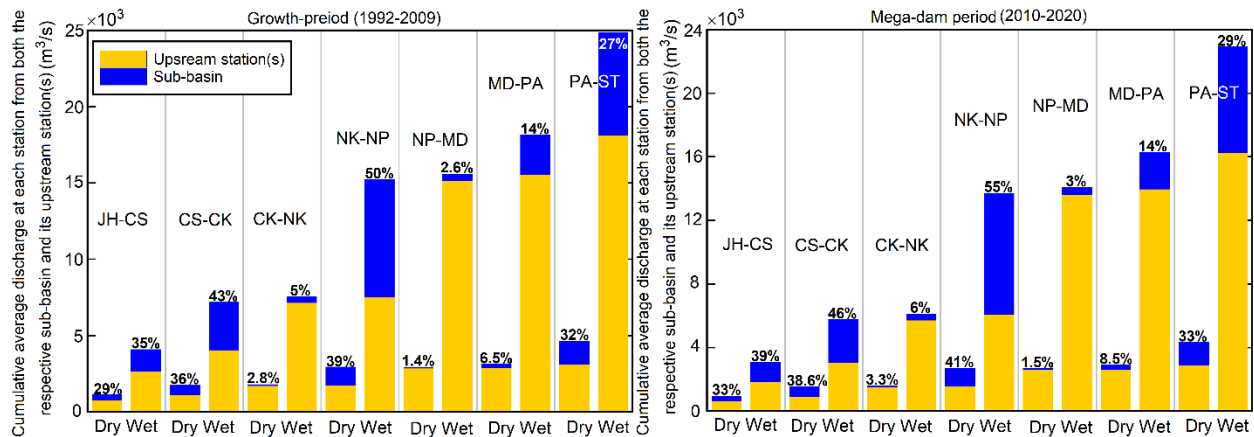
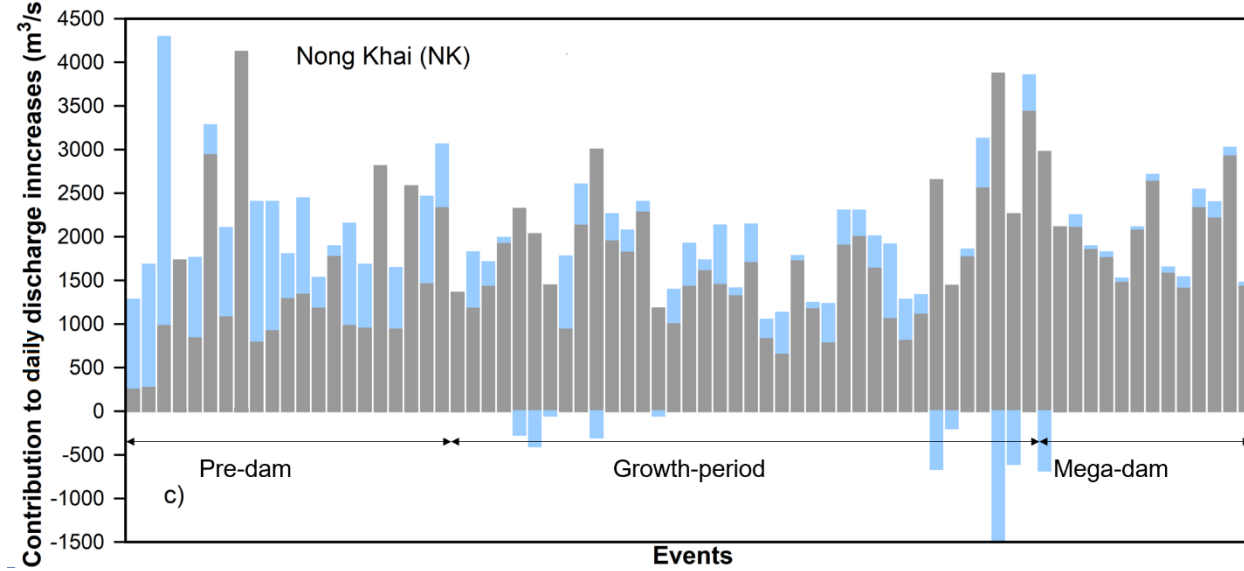
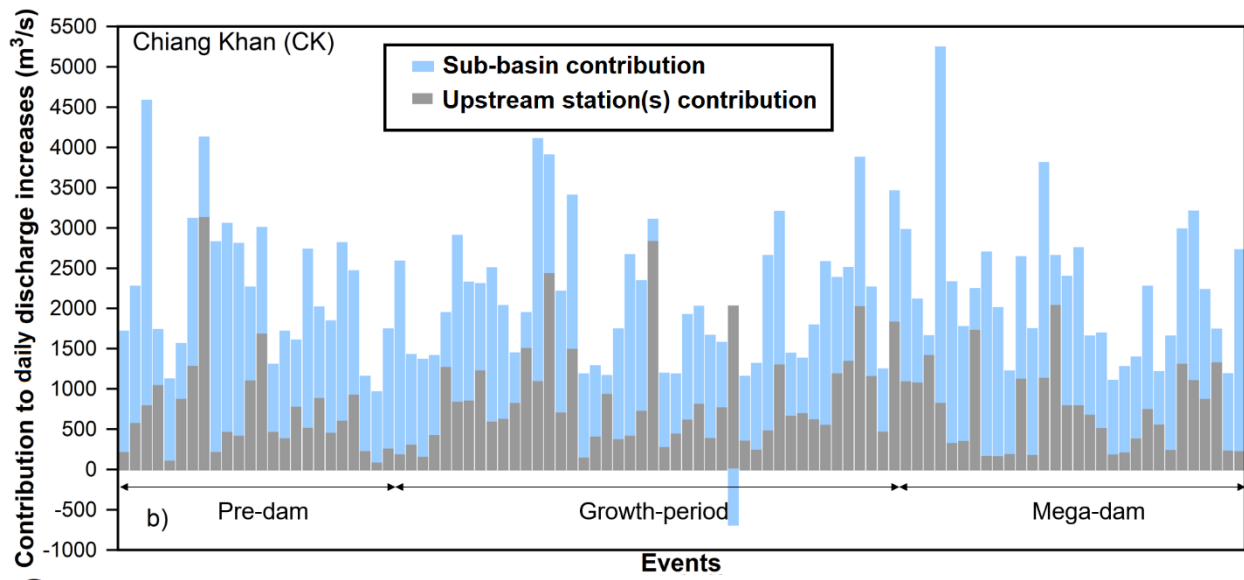


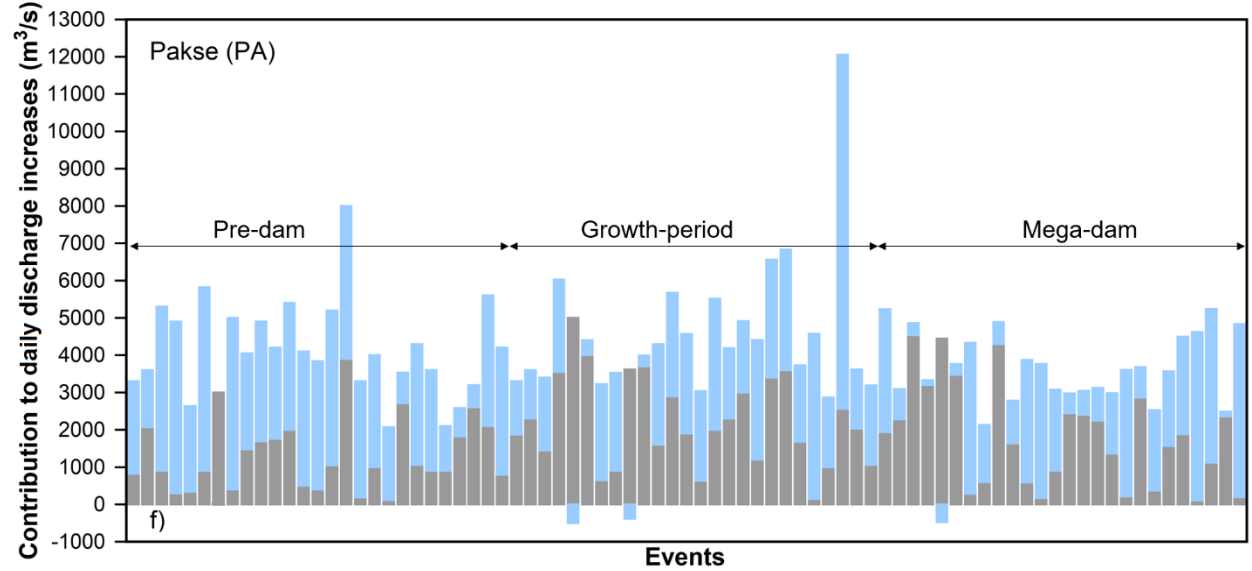
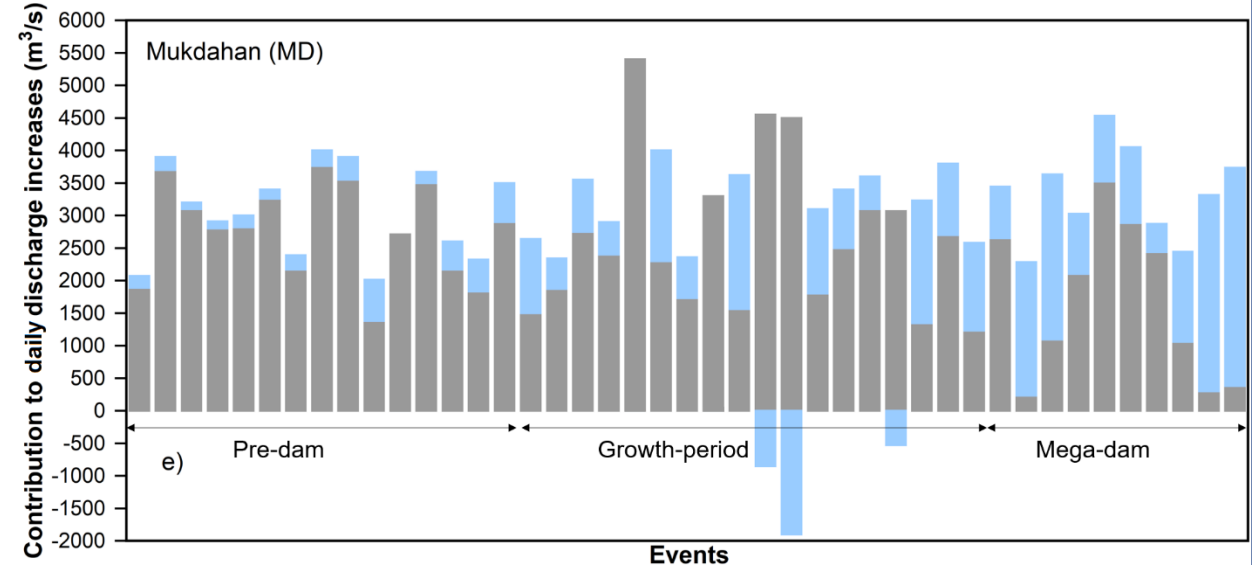
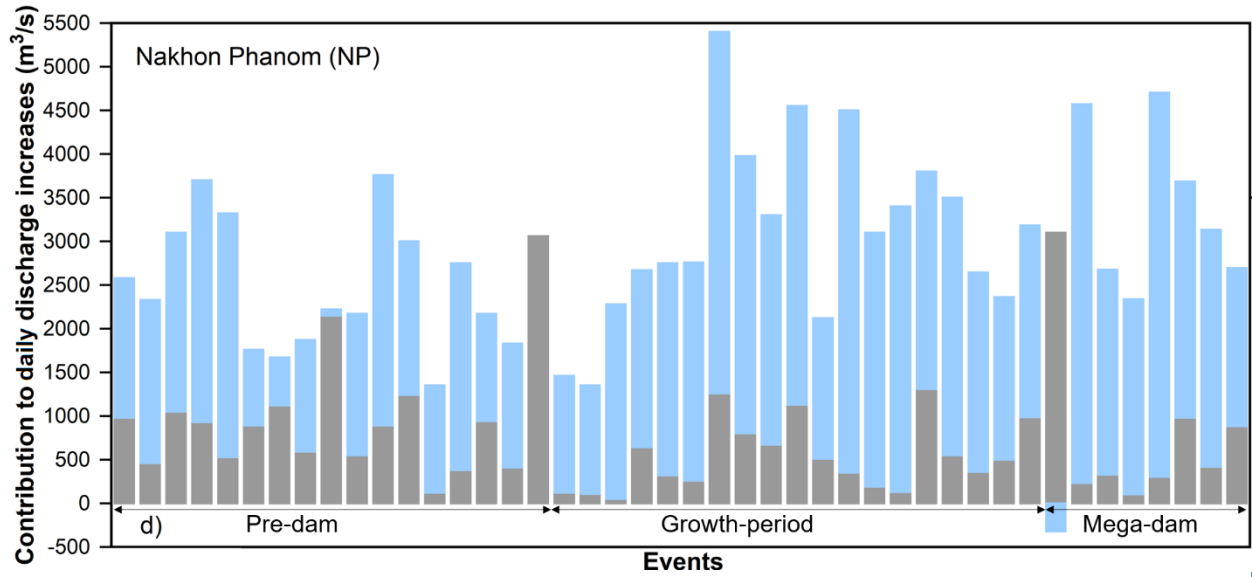
Figure S7: illustrates the contribution of defined sub-basins to the total discharge passing through their downstream station during the growth period and mega-dam periods.

### 8. Additional figures for each event resulting in daily water level increases for all stations

Figures S8a to g depict the analysis conducted for each event during the defined periods at each mainstream station. It is observed that Stung Treng (ST) has encountered the lowest number of daily river flow increases resulting in water level changes exceeding 1 meter. With the exception of Mukdahan (MD) and NongKhai (NK) stations, which are located close to their upstream station and have relatively small sub-basins compared to other stations, the contribution of other sub-basins to downstream large daily river flow increases is more significant.







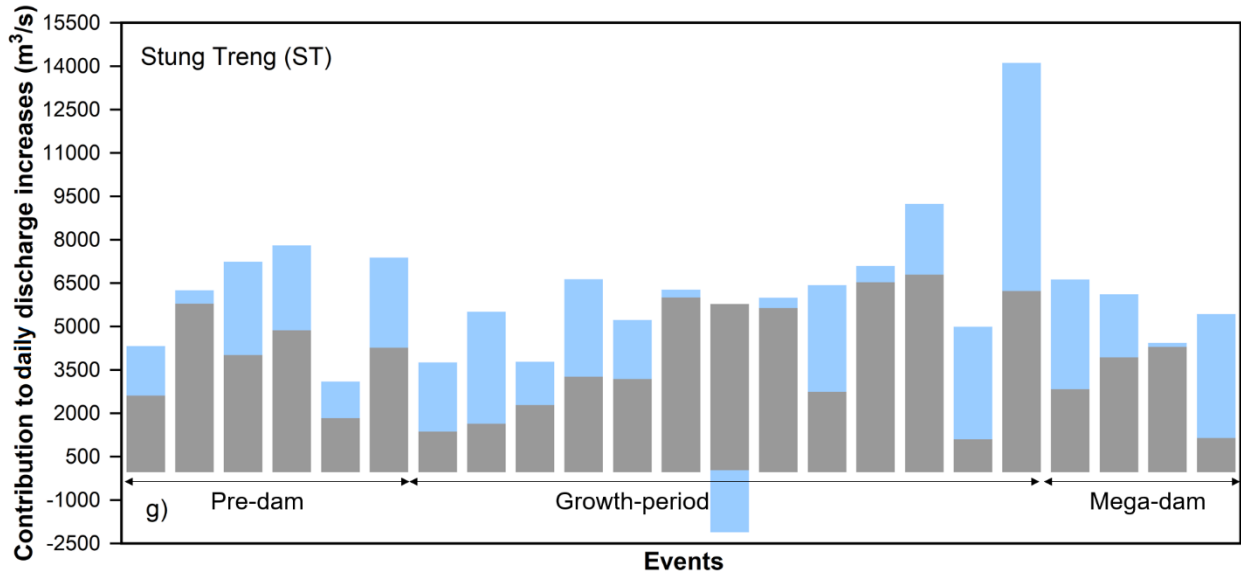


Figure S8. Event analysis for large daily river flow increases, leading to water level rises exceeding 1 meter, across the pre-dam period, growth period, and mega-dam period.

### 9. A figure for the precipitation trend

Figure S9 illustrates the estimated precipitation received in the JH-CS sub-basin during July 1986. Despite fluctuations, precipitation in this month exhibited a consistent upward trend until two notable river flow shifts, each exceeding a water level increase of >1m at the CS station. Analysis indicated that such patterns were frequent in the basin, potentially contributing to a higher occurrence of increased events compared to reduction events.

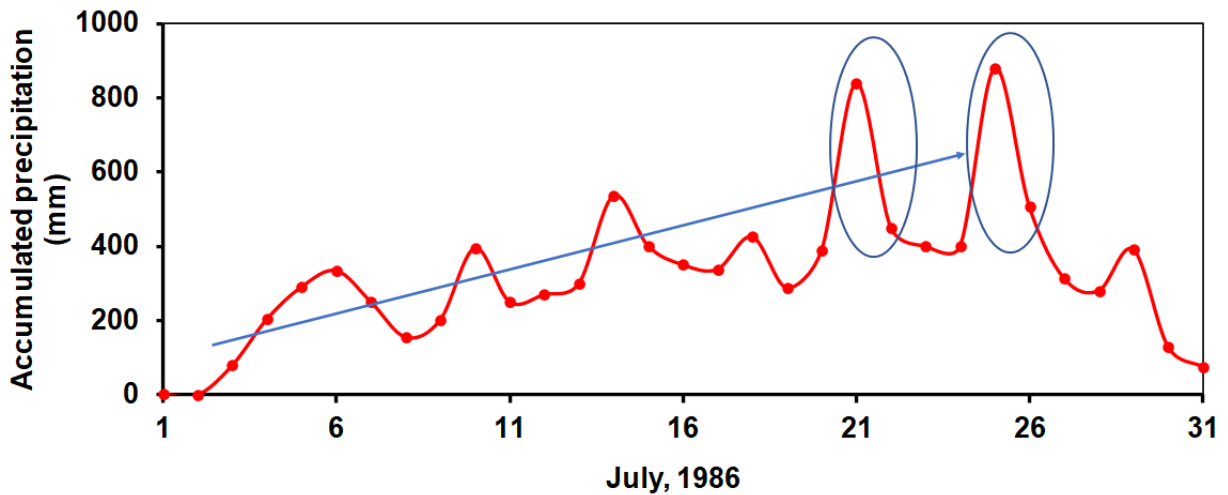


Figure S9. The trend of precipitation received in the JH-CS subbasin in July 1986 resulted in water level increases of greater than 1 m.